JCI insight

RESEARCH ARTICLE

PTHrP targets HDAC4 and HDAC5 to repress chondrocyte hypertrophy

Shigeki Nishimori,[1] Forest Lai,[1] Mieno Shiraishi,[1] Tatsuya Kobayashi,[1] Elena Kozhemyakina,[2] Tso-Pang Yao,[3] Andrew B. Lassar,[2] and Henry M. Kronenberg[1]

[1]Endocrine Unit, Massachusetts General Hospital and Harvard Medical School, Boston, Massachusetts, USA.

[2]Department of Biological Chemistry and Molecular Pharmacology, Harvard Medical School, Boston, Massachusetts, USA.

[3]Department of Pharmacology and Cancer Biology, Duke University School of Medicine, Durham, North Carolina, USA.

During endochondral bone formation, chondrocyte hypertrophy represents a crucial turning point from chondrocyte differentiation to bone formation. Both parathyroid hormone-related protein (PTHrP) and histone deacetylase 4 (HDAC4) inhibit chondrocyte hypertrophy. Using multiple mouse genetics models, we demonstrate in vivo that HDAC4 is required for the effects of PTHrP on chondrocyte differentiation. We further show in vivo that PTHrP leads to reduced HDAC4 phosphorylation at the 14-3-3–binding sites and subsequent HDAC4 nuclear translocation. The *Hdac4*-KO mouse shares a similar but milder phenotype with the *Pthrp*-KO mouse, indicating the possible existence of other mediators of PTHrP action. We identify HDAC5 as an additional mediator of PTHrP signaling. While the *Hdac5*-KO mouse has no growth plate phenotype at birth, the KO of *Hdac5* in addition to the KO of *Hdac4* is required to block fully PTHrP action on chondrocyte differentiation at birth in vivo. Finally, we show that PTHrP suppresses myocyte enhancer factor 2 (Mef2) action that allows runt-related transcription factor 2 (*Runx2*) mRNA expression needed for chondrocyte hypertrophy. Our results demonstrate that PTHrP inhibits chondrocyte hypertrophy and subsequent bone formation in vivo by allowing HDAC4 and HDAC5 to block the Mef2/Runx2 signaling cascade. These results explain the phenotypes of several genetic abnormalities in humans.

Introduction

Most of the vertebrate skeleton is generated by endochondral bone formation, in which growth plate chondrocytes direct subsequent bone formation (1). The developing growth plate has 3 morphologically distinct layers of chondrocytes: round chondrocytes, flat columnar chondrocytes, and hypertrophic chondrocytes (Supplemental Figure 1, A and B; supplemental material available online with this article; https://doi.org/10.1172/jci.insight.97903DS1) (2, 3). Round chondrocytes and flat columnar chondrocytes both proliferate in fetal life. Flat columnar chondrocytes increase their rate of proliferation an then stop proliferating and enlarge many fold to become hypertrophic chondrocytes. The fetal growth plate is surrounded by perichondrium, in which immature osteoblast precursors (cells expressing type II collagen [4], and then nestin [5] and osterix [6]) respond to signals from prehypertrophic and hypertrophic chondrocytes to become osteoblasts (Supplemental Figure 1B).

Parathyroid hormone-related protein (PTHrP, also known as parathyroid hormone–like [PTH-like] hormone [PTHLH]) was first recognized as a cause of high serum calcium in cancer patients (7). While PTHrP and PTH share homology only within the first 13 amino acids (8), they share a common receptor (9). The *Pthrp*-KO mouse dies immediately after birth from respiratory failure caused by a small circumference of the rib cage in association with extensive chondrocyte hypertrophy and mineralization that are not seen in normal rib cartilage (10), demonstrating an essential physiological role of PTHrP. PTHrP, synthesized by and secreted from round chondrocytes, suppresses chondrocyte hypertrophy (Supplemental Figure 1B). The PTH/PTHrP receptor–KO (PTH 1 receptor [PTH1R]) mouse resembles the *Pthrp*-KO mouse, with anterior rib chondrocyte hypertrophy and mineralization (11). In humans, fetuses with the absence of functional PTH/PTHrP receptor (Blomstrand chondrodysplasia) exhibit a phenotype similar to that of the *Pth1r*-KO mice (12). Further, the chondrocyte-specific *Pthrp*-Tg mouse that overexpresses human PTHrP protein using a mouse type 2 collagen promoter exhibits delayed

Conflict of interest: The authors have declared that no conflict of interest exists.

Submitted: October 5, 2017
Accepted: January 25, 2019
Published: March 7, 2019

Reference information:
JCI Insight. 2019;4(5):e97903.
https://doi.org/10.1172/jci.insight.97903.

chondrocyte hypertrophy in the growth plate (13). The heterozygous (HET) *Pthrp*-Tg (*Pthrp*-Tg/+) mouse has only round chondrocytes in all the long bones up to 1 week after birth, and subsequent bone formation is also severely delayed (Supplemental Figure 1C).

The class I histone deacetylase (HDAC) proteins (HDAC1, -2, -3, and -8) are ubiquitously expressed nuclear enzymes that exhibit HDAC activity. Histone deacetylation leads to chromatin condensation and subsequent transcriptional repression. In contrast, the class IIa HDAC proteins (HDAC4, -5, -7 and -9) are expressed in specific tissues and exhibit only minimum HDAC activity (14). In addition to the variant HDAC domain, the class IIa HDAC proteins have a characteristic N-terminal extension, with conserved binding sites for 14-3-3 proteins and for transcription factors, such as myocyte enhancer factor 2 (Mef2) (14). When bound by 14-3-3 proteins in the cytoplasm, the class IIa HDAC proteins do not block the transcriptional activity of Mef2 in the nucleus. Thus, the class IIa HDAC proteins, through release from 14-3-3 proteins and nuclear translocation, act as negative regulators of nuclear Mef2 (15). As expected from the crucial actions of Mef2 in skeletal and cardiac muscle, the KO mouse for the class IIa HDAC proteins, *Hdac5* (16), *Hdac7* (17), and *Hdac9* (18), exhibited cardiovascular phenotypes. However, the *Hdac4*-KO mouse unexpectedly exhibited a lethal phenotype in chondrocytes, characterized by rib chondrocyte hypertrophy and mineralization that do not occur in WT mice (19).

A subsequent mouse genetic study found that Mef2 induces chondrocyte hypertrophy (20). PTHrP regulation of the HDAC4/Mef2 interaction was then shown in an in vitro study using cultured chick primary chondrocytes (21). In humans, haploinsufficiency of *PTHRP* (22) or of *HDAC4* (23) causes the skeletal dysplasia, brachydactyly type E, suggesting a functional linkage between PTHrP and HDAC4. However, a direct test of this functional relationship has not been made in vivo.

In the present study, we demonstrate in vivo that HDAC4 is required for the effect of PTHrP on chondrocyte differentiation. We show in vivo that PTHrP action leads to lower HDAC4 phosphorylation and induces subsequent nuclear translocation of HDAC4 protein. However, our mouse models demonstrate that HDAC4 is not the sole mediator of PTHrP signaling. We identified HDAC5 as an additional mediator of PTHrP signaling in chondrocytes, though the *Hdac5*-KO mouse has no growth plate phenotype when HDAC4 is present. We further found that the actions of PTHrP on HDAC4 suppress Mef2 action; this action of Mef2 otherwise would allow runt-related transcription factor 2 (*Runx2*) expression that is needed for chondrocyte hypertrophy. We have thus identified a crucial signaling pathway that regulates chondrocyte differentiation in mice and humans.

Results

Accelerated chondrocyte differentiation in the Hdac4-KO skeleton is a milder form of that in the Pthrp-KO skeleton. If HDAC4 is a mediator of PTHrP signaling in chondrocytes, then the *Pthrp*-KO mouse and the *Hdac4*-KO mouse should exhibit a similar skeletal phenotype. We compared two representative regions of growth-associated chondrocytes: the growth plate in the proximal tibia and the anterior rib cartilage. In the newborn *Pthrp*-KO mouse, the distance from the top of the growth plate to the beginning of the hypertrophic layer (shown by black lines in Figure 1A) was extremely short due to the accelerated chondrocyte hypertrophy (Figure 1A, 35.3% of the WT controls). The *Hdac4*-KO mouse displayed a similar but milder phenotype at birth (Figure 1A, 64.1% of the WT controls).

The *Pthrp*-KO mouse died immediately after birth due to chondrocyte hypertrophy and mineralization in the anterior rib cartilage, where it is not normally found, and the consequent small rib cage (Figure 1A, black arrows). In contrast, the *Hdac4*-KO mouse had normal rib cartilage differentiation at birth (Figure 1A). Progressively accelerated rib chondrocyte hypertrophy starts at P2 (19). We observed the presence of widespread hypertrophic chondrocytes in the anterior rib cartilage of the *Hdac4*-KO mouse at P8 (Figure 1B, black arrows). Consistent with the progressive rib chondrocyte hypertrophy, the *Hdac4*-KO mouse died between P10 and P14. The phenotype similar to that of the *Pthrp*-KO mouse supports the hypothesis that HDAC4 mediates PTHrP signaling. However, the milder phenotype of the *Hdac4*-KO mouse also suggests the possible existence of other mediators of PTHrP signaling in the *Hdac4*-KO mouse.

The chondrocyte phenotype in the universal Hdac4-KO mouse depends only on HDAC4 KO in chondrocytes. To exclude the possibility that systemic effects caused by loss of HDAC4 in other organs have an important contribution to the chondrocyte phenotype in the universal *Hdac4*-KO mouse, we generated a chondrocyte/bone-specific conditional *Hdac4*-KO mouse using the type 2 collagen-*Cre* mouse (24) and the *Hdac4*-floxed mouse (25). The type 2 collagen-*Cre* that we used is active in chondrocytes and perichondrial cells, leading

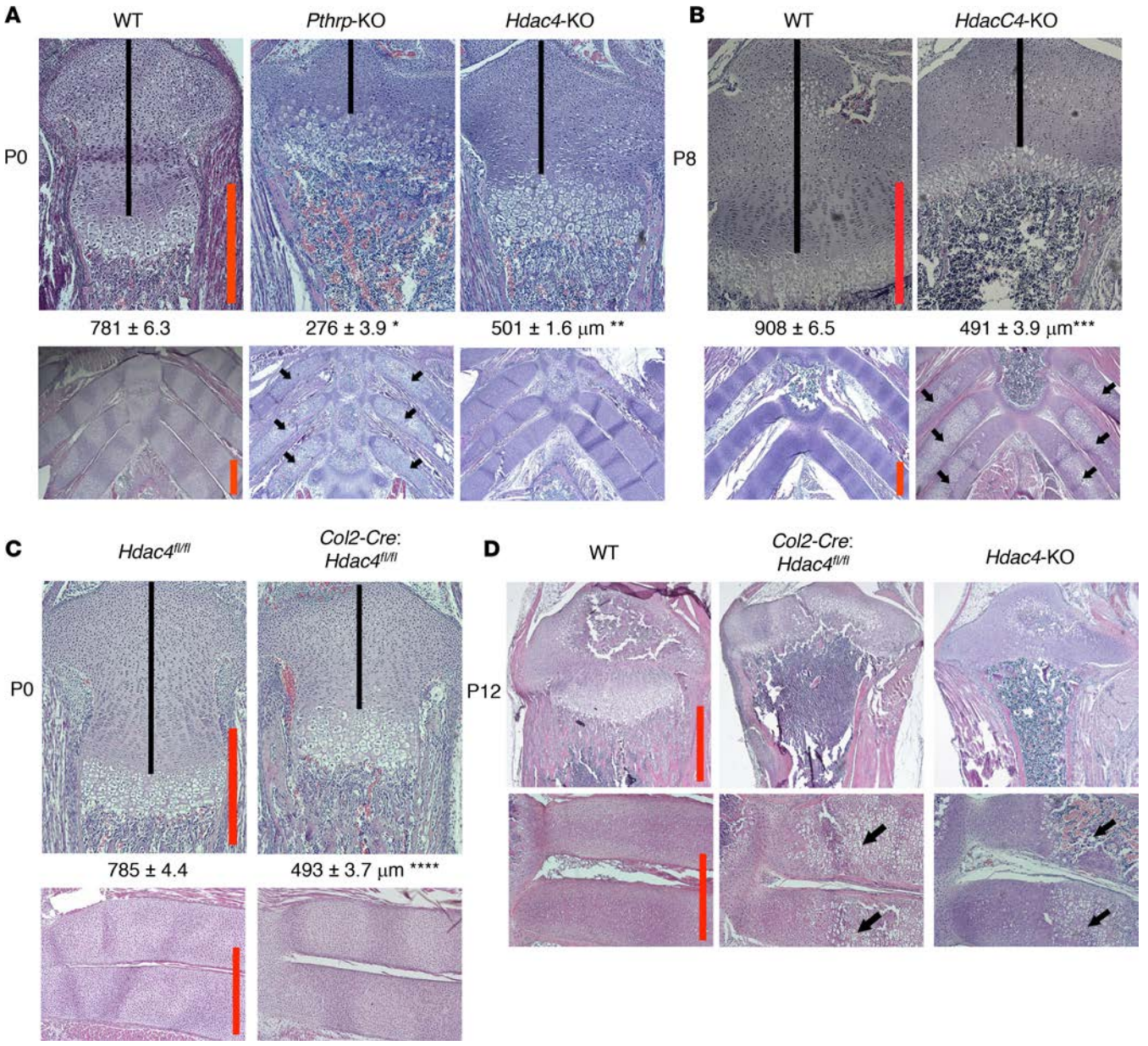

Figure 1. Accelerated chondrocyte differentiation in the *Hdac4*-KO skeleton is a milder form of that in the *Pthrp*-KO skeleton. H&E staining of the proximal tibial growth plate (original magnification, ×100 [**A**–**C**, top]; ×40 [**D**, top]), the anterior rib cage (original magnification, ×40 [**A** and **B**, bottom]), and the anterior rib cartilage (original magnification, ×100 [**C** and **D**, bottom]) at birth (**A** and **C**), P8 (**B**), and P12 (**D**). The mice with the same ages are littermates, except the *Hdac4*-KO mouse in **D**. To compare the *Pthrp*-KO mouse and the *Hdac4*-KO mouse precisely within the same litter, we mated the *Hdac4/Pthrp* double-HET mouse with the *Hdac4/Pthrp* double-HET mouse. (**A**). Numbers represent the average length of the proliferating chondrocyte region (shown by black lines) (mean ± SEM, $n = 3$, biological triplicates). *$P = 7 \times 10^{-7}$, **$P = 6 \times 10^{-6}$, ***$P = 8 \times 10^{-7}$, ****$P = 3 \times 10^{-6}$ by the 2-tailed Student's t test, when compared with its corresponding WT measurement. A P value of less than 0.05 was considered significant. Black arrows indicate rib chondrocyte hypertrophy and mineralization that do not occur in the WT controls. Scale bars (red lines): 500 μm.

to loss of *Hdac4* from chondrocytes and osteoblasts, and avoids widespread KO of *Hdac4* in other cell types. The chondrocyte/bone-specific conditional *Hdac4*-KO mouse (*Col2-Cre: Hdac4*$^{fl/fl}$) exhibited a shorter proliferating region in the tibial growth plate (Figure 1C, black lines, 62.8% of the *Hdac4*$^{fl/fl}$-controls) and normal rib cartilage (Figure 1C) at birth, as seen in the universal *Hdac4*-KO mouse (Figure 1A). At P12, both KO mice shared a similar phenotype with the newborn *Pthrp*-KO mouse: extremely short tibial growth plate and extensive rib chondrocyte hypertrophy and mineralization that are not seen in the WT control (Figure 1D, black arrows). The *Col2-Cre: Hdac4*$^{fl/fl}$ mouse died around P14, as seen in the universal *Hdac4*-KO mouse. We next generated a late chondrocyte/bone-specific conditional *Hdac4*-KO mouse using the *Osterix-*

Cre (*Osx*-Cre) mouse (26). The *Osx*-Cre that we used is active in hypertrophic chondrocytes, perichondrium, and osteoblasts. In contrast to the *Col2-Cre:Hdac4*$^{fl/fl}$ mouse, the *Osx-Cre:Hdac4*$^{fl/fl}$ mouse exhibited a normal phenotype in the growth plates and bones (Supplemental Figure 2). The *Osx-Cre: Hdac4*$^{fl/fl}$ mouse can survive until adulthood with a normal body. This result demonstrates that the chondrocyte phenotype in the universal *Hdac4*-KO mouse depends only on proliferating chondrocytes.

We did not obtain this straightforward result with our initial experiments. At the fifth generation of backcrossing of the original *Hdac4*-floxed mice (mixed genetic background) to the C57BL/6 mice, the chondrocyte-specific conditional *Hdac4*-KO mice showed a clear phenotype only in the growth plate chondrocytes of the limbs but not in the rib chondrocytes. We could observe the rib phenotype only after we backcrossed for 10 generations. This finding emphasizes the importance of uniform genetic background when interpreting the effects of specific mutations.

PTHrP and HDAC4 work through a common pathway. To examine whether PTHrP and HDAC4 work through a common pathway, we next analyzed the mouse doubly HET for *Pthrp* and *Hdac4*. Both single HET mice have growth plates of normal length (Figure 2A, black lines). If PTHrP and HDAC4 work independently, then the double-HET mouse should also have a normal growth plate. However, the double-HET mouse showed a significantly shorter proliferating region (Figure 2A, black line, 85.4% of the WT controls), which could result from lower PTHrP action in the growth plate. The phenotype of the double-HET mouse was mild but nevertheless similar to that of the individual KO mice (Figure 1A). This experiment indicates that PTHrP and HDAC4 repress chondrocyte hypertrophy though a common pathway.

As a more stringent genetic test of whether PTHrP action requires HDAC4 activity, we deleted the *Hdac4* gene in the *Pthrp*-Tg/+ mouse. If HDAC4 mediates PTHrP signaling, the *Hdac4* deletion should modify the PTHrP-Tg phenotype. Even the HET deletion of *Hdac4* partially blocks the PTHrP-Tg phenotype at birth (Figure 2B, *Hdac4*-HET: *Pthrp*-Tg/+ mouse). The tibia was 50% longer than that of the *Pthrp*-Tg/+ mouse, and we observed flat columnar chondrocytes and hypertrophic chondrocytes in the tibia (Figure 2B, black arrow), findings that do not occur in the *Pthrp*-Tg/+ mouse at birth. These findings were confirmed by ISH for Indian Hedgehog mRNA (Ihh, a gene expressed in prehypertrophic and early hypertrophic chondrocytes) and type 10 collagen mRNA (Col10a1, a gene expressed in hypertrophic chondrocytes) (Figure 2C).

Strikingly, the homozygous deletion of *Hdac4* almost completely reversed the PTHrP-Tg phenotype. Unlike the *Pthrp*-Tg/+ control, the *Hdac4*-KO: *Pthrp*-Tg/+ mouse exhibited a distinct growth plate, bone, bone marrow, and a tibia of normal length at birth (Figure 2B). This result clearly demonstrates that HDAC4 is required to mediate PTHrP signaling. However, the *Hdac4*-KO: *Pthrp*-Tg/+ mouse is not exactly the same as the *Hdac4*-KO mouse, as would be expected if HDAC4 were the sole mediator of PTHrP signaling. The *Hdac4*-KO: *Pthrp*-Tg/+ mouse exhibited an extremely long hypertrophic layer (Figure 2B, black line) and a longer tibia than the *Hdac4*-KO mouse at birth, suggesting that PTHrP must induce these differences through other mediators.

At E17.5 we saw more obvious differences between the *Hdac4*-KO mouse and the *Hdac4*-KO: *Pthrp*-Tg/+ mouse. The longer proliferating zone in the *Hdac4*-KO: *Pthrp*-Tg/+ mouse (Supplemental Figure 3, black line) represents delayed chondrocyte hypertrophy due to greater PTHrP action through mediators other than HDAC4. In the *Hdac4*-KO: *Pthrp*-Tg/+ mouse, the hypertrophic region occupied the central region and bone formation started from both perichondria (Supplemental Figure 3, black arrows). The long hypertrophic layer in the *Hdac4*-KO: *Pthrp*-Tg/+ mouse at birth probably reflects the earlier delay in the separation of the hypertrophic regions.

We wanted to exclude an alternative explanation of our findings — if the deletion of *Hdac4* lowered the activity of the type 2 collagen promoter in the *Pthrp*-Tg/+ mouse, then the consequent reduced PTHrP overexpression might lead to the observed phenotypes. To exclude this possibility, we examined *Pthrp* mRNA expression levels by ISH. The *Pthrp*-Tg/+ mouse overexpressed human PTHrP (amino acids 1–141) protein (13). The human PTHrP (amino acids 1–141) region has 7 mismatches with mouse PTHrP in the amino acid sequence but has 55 mismatches in the DNA sequence. Because our mouse *Pthrp* cRNA probe did not detect human *Pthrp* mRNA in the *Pthrp*-Tg/+ mouse, we generated a human *Pthrp* cRNA probe. Then, we confirmed that the HET or homozygous deletion of *Hdac4* did not lower the human *Pthrp* mRNA overexpression in the proliferating chondrocytes (Figure 2D). Thus, our results are most consistent with a model in which the *Hdac4* deletion blocks the actions of PTHrP.

PTHrP signaling reduces HDAC4 phosphorylation. To investigate the molecular mechanisms underlying the effects of PTHrP signaling on HDAC4, we examined in vivo whether PTHrP regulates the phosphory-

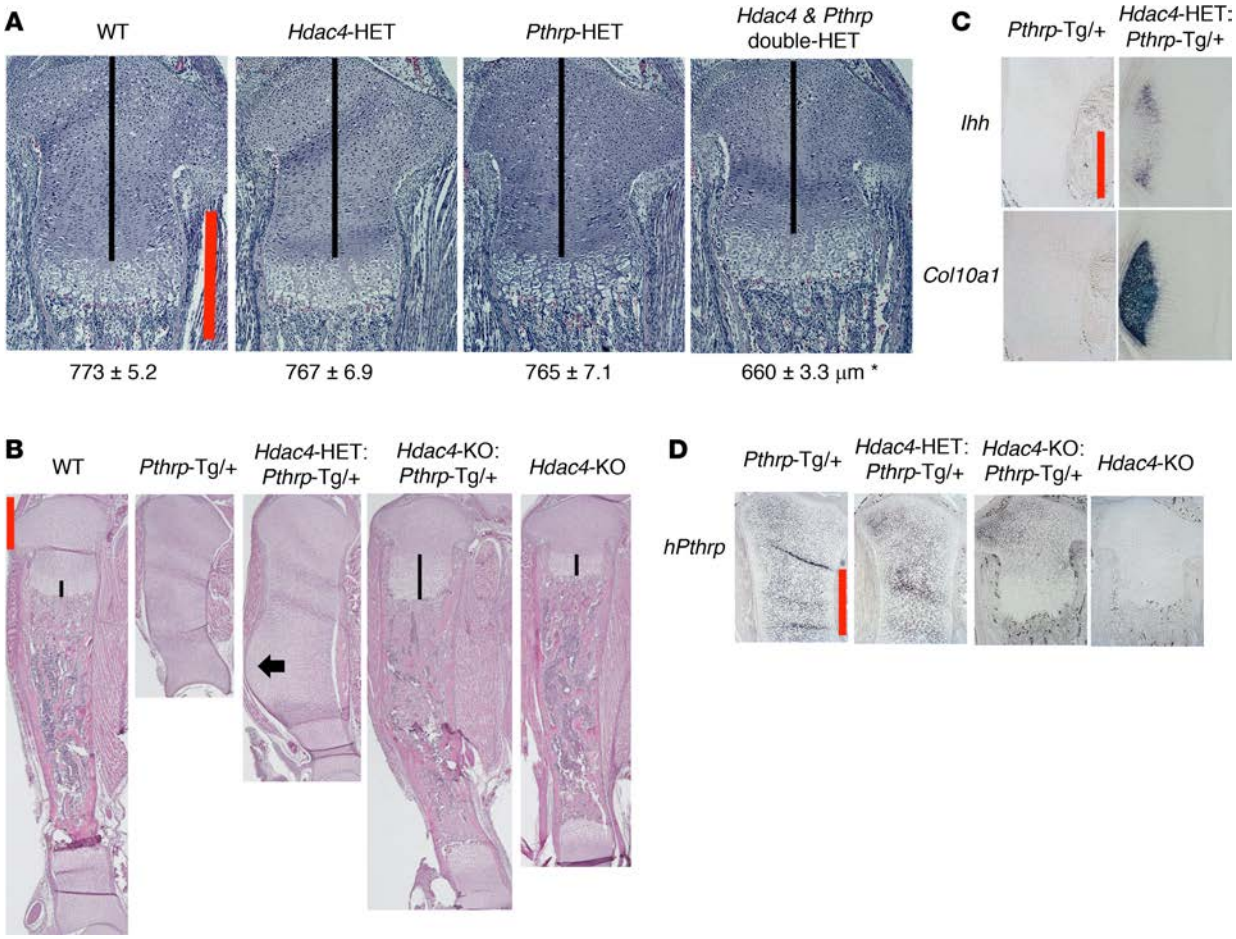

Figure 2. PTHrP and HDAC4 work through a common pathway. (**A**) H&E staining of the proximal tibial growth plate at birth (original magnification, ×100). The mice shown are littermates. Numbers represent the average length of the proliferating chondrocyte region (shown by black lines) (mean ± SEM, $n = 3$, biological triplicates). *$P < 0.0003$ by random intercept linear mixed-effects model (SAS Institute). A P value of less than 0.05 was considered significant. (**B**) H&E staining of the whole tibia at birth (original magnification, ×20). The mice shown are littermates from mating between the *Hdac4*-HET mouse and the *Hdac4*-HET-*Pthrp*-Tg/+ mouse. Black arrow indicates the flat columnar and hypertrophic chondrocyte region. Black lines indicate the length of hypertrophic chondrocyte layer. The reproducibility of the phenotype was confirmed by 3 independent litters. (**C** and **D**) ISH for *Ihh* mRNA and *Col10a1* mRNA at the medial tibia and for human *Pthrp* mRNA at the proximal tibial growth plate (original magnification, ×100). Same mice as shown in **B**. Scale bars (red lines): 500 μm.

lation status of HDAC4 protein at three 14-3-3–binding sites. A previous in vitro study using overexpressed HDAC4 protein in chick primary chondrocytes demonstrated that acute treatment with either PTHrP or forskolin leads to markedly decreased phosphorylation of HDAC4 protein specifically at the first 14-3-3–binding site, while phosphorylation at the other two sites was not significantly altered (21). To analyze PTHrP action in vivo, we manually microdissected proliferating chondrocytes from the proximal tibial growth plates at birth (see Methods), and then we examined the degree of HDAC4 phosphorylation by Western blots, using antibodies that detect the site-specific phosphorylation (21, 27)

The first antibody we used recognizes the first phospho-HDAC site on HDAC4 (Ser246), HDAC5 (Ser259), andHDAC7 (Ser155) (the indicated residues represent those in the human HDAC4 protein). The residues in mouse HDAC4 protein are HDAC4 (Ser245), HDAC5 (Ser250), and HDAC7 (Ser178)). This antibody detects 2 bands on Western blots of chondrocytes from the proliferative region of the growth plate at birth (Figure 3, A and C). Recently, the manufacture (Cell Signaling Technology) changed the assignment of the upper band from phospho-HDAC4 (Ser246) alone to a combination of phospho-HDAC4 (Ser246) and phosho-HDAC5 (Ser259). In our laboratory, we have confirmed these new assignments using analogous Western blots from an HDAC4- and HDAC5-ablated osteocyte cell line (T. Sato and M. Wein, unpublished data).

First, we compared the phosphorylation of the first 14-3-3–binding site among the *Pthrp*-Tg/+ mouse, the *Pthrp*-KO mouse, and their WT controls. Though we cannot analyze the phosphorylated HDAC4

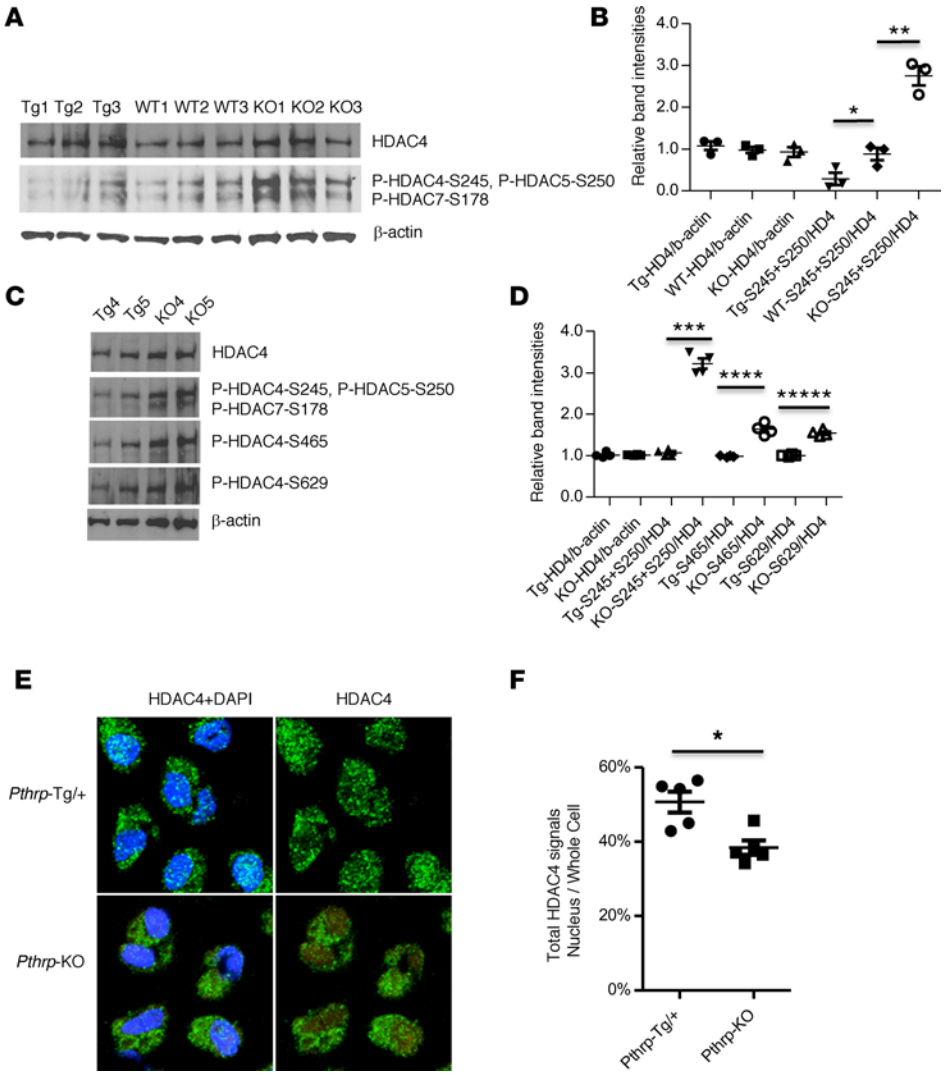

Figure 3. HDAC4 dephosphorylation and nuclear translocation by PTHrP signaling in vivo. (**A** and **C**) Western blots for the 14-3-3–binding sites (see complete unedited blots in the supplemental material). Whole cell lysate from microdissected proliferating chondrocyte regions in the proximal tibial growth plates at birth. Different sets of animals were used (**A**, $n = 3$, biological triplicates; **C**, $n = 2$, biological duplicates). Tg, *Pthrp*-Tg/+; KO, *Pthrp*-KO. WT1 or WT2 and WT3 are derived from Tg litter or KO litter, respectively (**A**). Tg1 and Tg2 are littermates. The KO pups are derived from different litters. (**B** and **D**) Relative band intensities were calculated from the bands in **A** ($n = 3$) or **C** ($n = 2$) as well as Supplemental Figure 4A ($n = 2$). HDAC4 was normalized to β-actin. Phosphorylated HDACs were normalized to HDAC4. S245+S250, the sum of phospho HDAC4-Ser245 and phospho HDAC5-Ser250; S465, phospho HDAC4-Ser465; S629, phospho HDAC4-Ser629. $^{*}P = 0.03$, $^{**}P = 0.002$, $^{***}P = 1 \times 10^{-5}$, $^{****}P = 4 \times 10^{-4}$, $^{*****}P = 5 \times 10^{-5}$ by the 2-tailed Student's *t* test. (**E**) Representative IHC images by confocal microscopy (original magnification, ×620). Round chondrocytes in the proximal tibial growth plates at birth: green (HDAC4) and blue (DAPI, nuclear stain). (**F**) Average ratio of total HDAC4 intensities in nuclei to those in whole cells (mean ± SEM, $n = 5$, biological replicates). The ratio for *Pthrp*-Tg/+ cells was 50.7% ± 2.4% and for *Pthrp*-KO cells was 38.4% ± 1.3%. The detailed calculation is shown in Supplemental Figure 4B and Supplemental Table 1. $^{*}P < 0.0001$ by random intercept linear mixed-effects model (SAS Institute). A *P* value of less than 0.05 was considered significant (**B**, **D**, and **F**).

(Ser245) alone, we observed the significantly reduced phosphorylation levels of HDAC4 (Ser245) and HDAC5 (Ser250) at the first 14-3-3–binding site in the *Pthrp*-Tg/+ mouse compared with the levels in the WT controls (Figure 3, A and B; $P = 0.03$), a finding consistent with that in our previous in vitro study (21). HDAC4 phosphorylation at this site is significantly higher in the *Pthrp*-KO mouse compared with that in the WT controls (Figure 3, A and B; $P = 0.03$). The total HDAC4 protein levels were not altered among *Pthrp*-Tg/+, *Pthrp*-KO, and their WT controls (Figure 3, A and B).

Next, we compared HDAC4 phosphorylation levels at all the 14-3-3–binding sites between the *Pthrp*-

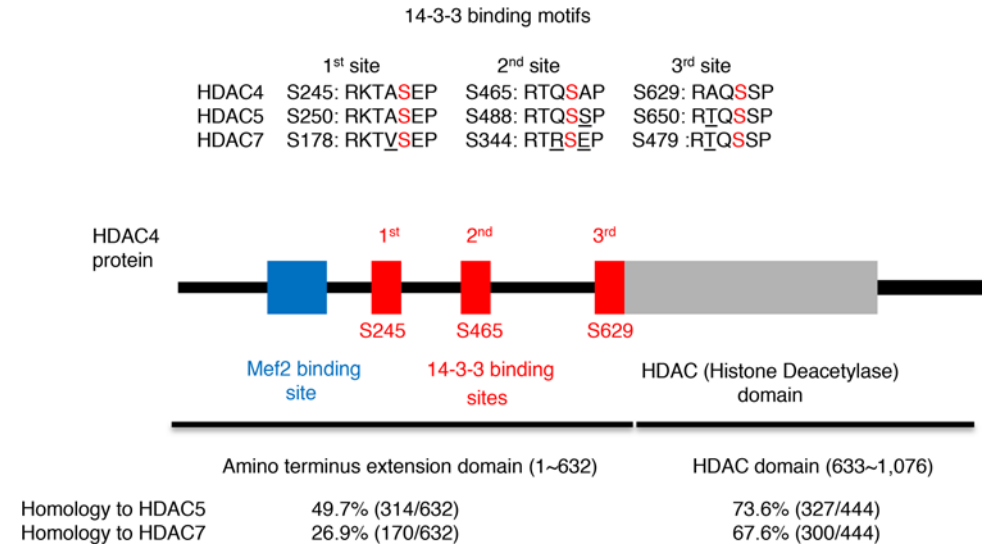

Figure 4. HDAC5 as a candidate to complement HDAC4 action. (Top) Homology of 14-3-3–binding motifs among HDAC4, HDAC5, and HDAC7 proteins. The red letter "S" represents phosphorylated serine. The underlined letters represent the mismatched amino acids. Theses motifs are conserved between mouse and human, except HDAC7-S479 (RAQSSP in human with one mismatch). (Middle) Protein domains of HDAC4. (Bottom) Homology of HDAC4 protein to HDAC5 or HDAC7 in the N-terminal extension domain or in the C-terminal HDAC domain. The protein sequences were analyzed by Clustal Omega, a multiple sequence alignment program.

Tg/+ mouse and the *Pthrp*-KO mouse at birth. We prepared 4 sets of *Pthrp*-Tg/+ mice (Tg4, Tg5, Tg6, and Tg7) and *Pthrp*-KO (KO4, KO5, KO6, and KO7) mice for the statistical analyses (Tg4–Tg7 and KO4–KO7: $n = 4$, biological replicate). We observed the most reduced HDAC4 phosphorylation at the first 14-3-3–binding site in the *Pthrp*-Tg/+ mouse, while we also detected lower levels of HDAC4 phosphorylation at the second and third binding sites (HDAC4 (Ser465) and HDAC4 (Ser629) (Ser467 and Ser632 in human HDAC4 protein, respectively) (Figure 3C and Supplemental Figure 4A).

To calculate the average band intensities, we performed 2 independent Western blots for these 8 samples. Total HDAC4 protein levels were not altered by PTHrP status when they were normalized to the levels of β-actin (Figure 3D). By normalizing the levels of phosphorylated HDAC4 protein to that of total HDAC4 protein, we found the most significant changes at the first 14-3-3–binding site, but the changes at the other two sites were also significant (Figure 3D). This result demonstrates that PTHrP signaling leads to reduced levels of HDAC4 phosphorylation at three 14-3-3–binding sites in vivo.

PTHrP signaling promotes HDAC4 nuclear translocation. When intracellular signals lead to a decrease in the level of phosphorylation of the 14-3-3–binding sites, the class IIa HDAC proteins are released from 14-3-3 proteins and then move into the nucleus (21). To demonstrate HDAC4 nuclear translocation induced by PTHrP signaling in vivo, we compared the intracellular HDAC4 localization between the *Pthrp*-Tg/+ mouse and the *Pthrp*-KO mouse by IHC, focusing on round proliferating chondrocytes in the proximal tibial growth plate at birth. Using confocal microscopy, we observed intense nuclear HDAC4 signals in the *Pthrp*-Tg/+ mouse. In contrast, HDAC4 signals appear lower in nuclei but higher in the cytoplasm in the *Pthrp*-KO mouse (Figure 3E).

For a quantitative assessment of the intracellular localization of HDAC4 protein, we established a method to calculate HDAC4 signal intensities in the nuclei and those in the whole cells by 3-color IHC (for HDAC4, nuclei, and whole cell) (see Methods, Supplemental Figure 4B, and Supplemental Table 1). We analyzed confocal images of the round proliferating chondrocytes in the proximal tibial growth plate (Supplemental Table 1; total cell number analyzed: Tg = 5,468, KO = 4,692) using 5 sets of the *Pthrp*-Tg/+ mice (Tg8, Tg9, Tg10, Tg11, and Tg12) and the *Pthrp*-KO mice (KO8, KO9, KO10, KO11, and KO12) at birth (Tg8–Tg12 and KO8–KO12: $n = 5$, biological replicates). The average ratio of total HDAC4 signal intensities in the nuclei to those in the whole cells was significantly higher in the *Pthrp*-Tg/+ mouse (Figure 3F, *Pthrp*-Tg/+: *Pthrp*-KO = 50.7% vs. 38.4%; $P < 0.0001$), supporting the hypothesis that PTHrP increases HDAC4 nuclear translocation.

Table 1. Gene expression levels in the 3 layers of the growth plate at birth

	Round cells	Flat cells	Hypertrophic cells
Hdac4	1.180	0.642	0.520
Hdac5	2.413	1.714	1.906
Hdac7	1.159	0.843	0.946
Hdac9	0.402	0.295	0.266
Pthrp	0.867	0.213	0.124
Col10a1	0.140	0.785	15.379
Col2a1	40.192	25.915	22.927
Mef2C	7.998	15.165	15.643
Runx2	1.129	5.831	7.958
β-Actin	56.581	61.577	61.521

mRNA expression levels by Affymetrix GeneChip in the 3 layers of the proximal tibial growth plates in WT Black Swiss mice at birth. The biological triplicate data were normalized and combined. Each layer was manually microdissected from the unfixed and fresh-frozen cryosections. The successful separation of each layer was confirmed by differential expression of *Pthrp* and *Col10a1*.

Identification of HDAC5 as an additional mediator of PTHrP signaling in chondrocytes. To identify additional mediators of PTHrP signaling that might work in the *Hdac4*-KO mouse, we focused on other class IIa HDAC proteins, namely HDAC5, HDAC7, and HDAC9. We hypothesized that the common N-terminal extension among the class IIa HDAC proteins might be regulated by PTHrP signaling, as we observed with HDAC4 (Figure 3 and Supplemental Figure 4A).

In microarray analysis using manually microdissected proximal tibial growth plates of newborn WT mice (see Methods), *Hdac5* mRNA and *Hdac7* mRNA showed similar expression levels to those of *Hdac4* mRNA, but the expression levels of *Hdac9* mRNA were at background levels (Table 1).

Then, we analyzed the homology of HDAC4 protein to HDAC5 or HDAC7. First, we focused on the conservation of the 14-3-3–binding motifs (Figure 4, top). Between HDAC4 and HDAC5, we found a perfect match at the first binding site and one mismatch at the second or the third binding site. Between HDAC4 and HDAC7, we found two more mismatches: one mismatch at the first or the third binding site and two mismatches at the second binding site (Figure 4). We also analyzed the homology in the whole N-terminal extension domain that is characteristic for class II HDAC family proteins. We found higher homology between HDAC4 and HDAC5 than between HDAC4 and HDAC7 (49.7% vs. 26.9%) in contrast to the similarity in the C-terminal HDAC domain (73.6% vs. 67.6%) (Figure 4, bottom). Taken together, we investigated HDAC5 first, which has higher homology to HDAC4 in protein sequence compared with HDAC7.

We first analyzed the *Hdac5*-KO mouse at birth but found a normal phenotype in the rib chondrocytes, tibial growth plate, and whole tibia (Figure 5, A and C), a finding consistent with the previous report showing normal growth of the *Hdac5*-KO mouse (16). Next, we analyzed mice with mutations in both *Hdac4* and *Hdac5*. Surprisingly, the *Hdac4*-KO: *Hdac5*-HET (4KO: 5HET) mouse died immediately after birth. The rib phenotype of this mouse was similar to that of the *Pthrp*-KO mouse, with dramatically accelerated chondrocyte hypertrophy (Figure 5A). This finding is consistent with the notion that HDAC5 mediates PTHrP signaling to suppress chondrocyte hypertrophy in the *Hdac4*-KO mouse. The *Hdac4* and *Hdac5* double-KO mouse died at birth with a more severe rib phenotype than that of the *Pthrp*-KO mouse (Figure 5A) and thus had a phenotype similar to that of the *PTH/PTHrP receptor*-KO mouse (28). The phenotype in the *Hdac4* and *Hdac5* double-KO mouse supports the hypothesis that both of these class II HDAC proteins are necessary for PTHrP signaling to efficiently block the initiation of chondrocyte hypertrophy.

ISH for marker genes in hypertrophic chondrocytes clearly provides molecular data that demonstrate the effects of *Hdac5* deletion in the *Hdac4*-KO mouse. The newborn *Hdac4*-KO mouse and WT mouse do not express *Col10a1* mRNA in anterior rib cartilage. However, the HET deletion of *Hdac5* in the *Hdac4*-KO mouse leads to *Col10a1* mRNA expression that resembles that of the *Pthrp*-KO mouse (Figure 5B, *Hdac4*-KO: *Hdac5*-HET and *Pthrp*-KO, black arrows). The double-KO mouse shows lower *Col10a1* mRNA expression but higher expression of osteopontin (*OPN*) mRNA (Supplemental Figure 5A, black arrows), as is seen in the PTH/PTHrP receptor–KO mouse, indicating further differentiation into the late hypertrophic stage, in which *OPN* mRNA is expressed. In contrast, *Col2a1* mRNA, expressed in proliferating

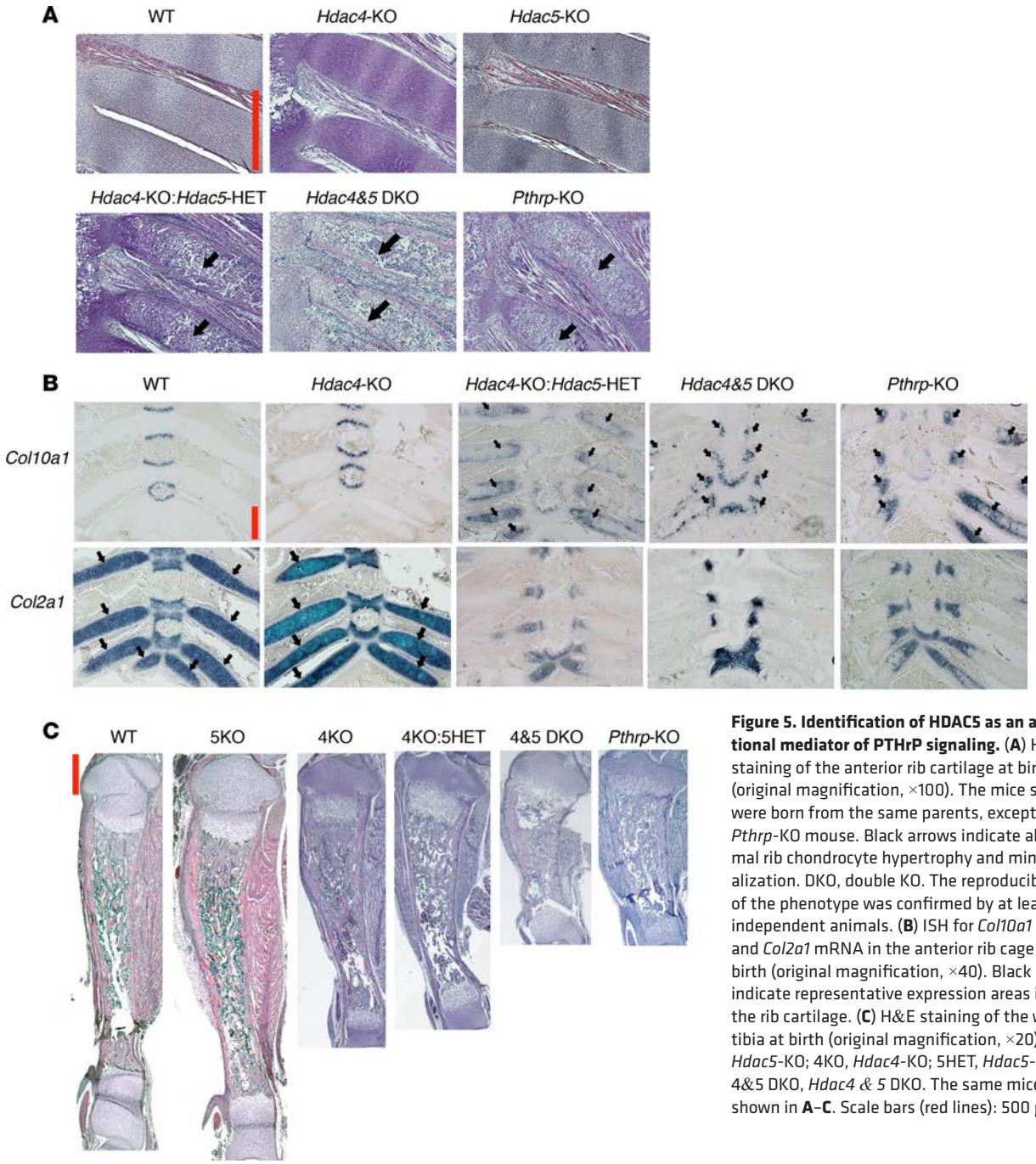

Figure 5. Identification of HDAC5 as an additional mediator of PTHrP signaling. (**A**) H&E staining of the anterior rib cartilage at birth (original magnification, ×100). The mice shown were born from the same parents, except the *Pthrp*-KO mouse. Black arrows indicate abnormal rib chondrocyte hypertrophy and mineralization. DKO, double KO. The reproducibility of the phenotype was confirmed by at least 2 independent animals. (**B**) ISH for *Col10a1* mRNA and *Col2a1* mRNA in the anterior rib cage at birth (original magnification, ×40). Black arrows indicate representative expression areas in the rib cartilage. (**C**) H&E staining of the whole tibia at birth (original magnification, ×20). 5KO, *Hdac5*-KO; 4KO, *Hdac4*-KO; 5HET, *Hdac5*-HET; 4&5 DKO, *Hdac4 & 5* DKO. The same mice are shown in **A**–**C**. Scale bars (red lines): 500 μm.

chondrocytes, showed high expression in anterior rib cartilage in both the WT mouse and the *Hdac4*-KO mouse (Figure 5B, black arrows). The HET or homozygous deletion of *Hdac5* in the *Hdac4*-KO mouse caused a dramatic decrease in *Col2a1* mRNA expression, just as seen in the *Pthrp*-KO mouse (Figure 5B).

The long bone phenotype in the *Hdac4*-KO: *Hdac5*-HET mouse was milder than that of the *Pthrp*-KO mouse, but the *Hdac4* and *Hdac5* double-KO mouse showed a phenotype similar to that of the *Pthrp*-KO mouse at birth (Figure 5C) and E18.5 (Supplemental Figure 5B).

HDAC5 mediates PTHrP signaling when HDAC4 expression is low. We further explored the relative actions of HDAC4 and HDAC5 in the setting of PTHrP overexpression in the growth plate. We first deleted the *Hdac5* gene in the *Pthrp*-Tg/+ mouse. The HET or homozygous deletion of *Hdac5* had no effects on the *Pthrp*-Tg/+ phenotype (Figure 6A), in contrast to the findings with the *Hdac4* deletion in the *Pthrp*-Tg/+ mouse (Figure 2, B and C). Next, we deleted the *Hdac5* gene in the *Hdac4*-HET: *Pthrp*-Tg/+ mouse. With

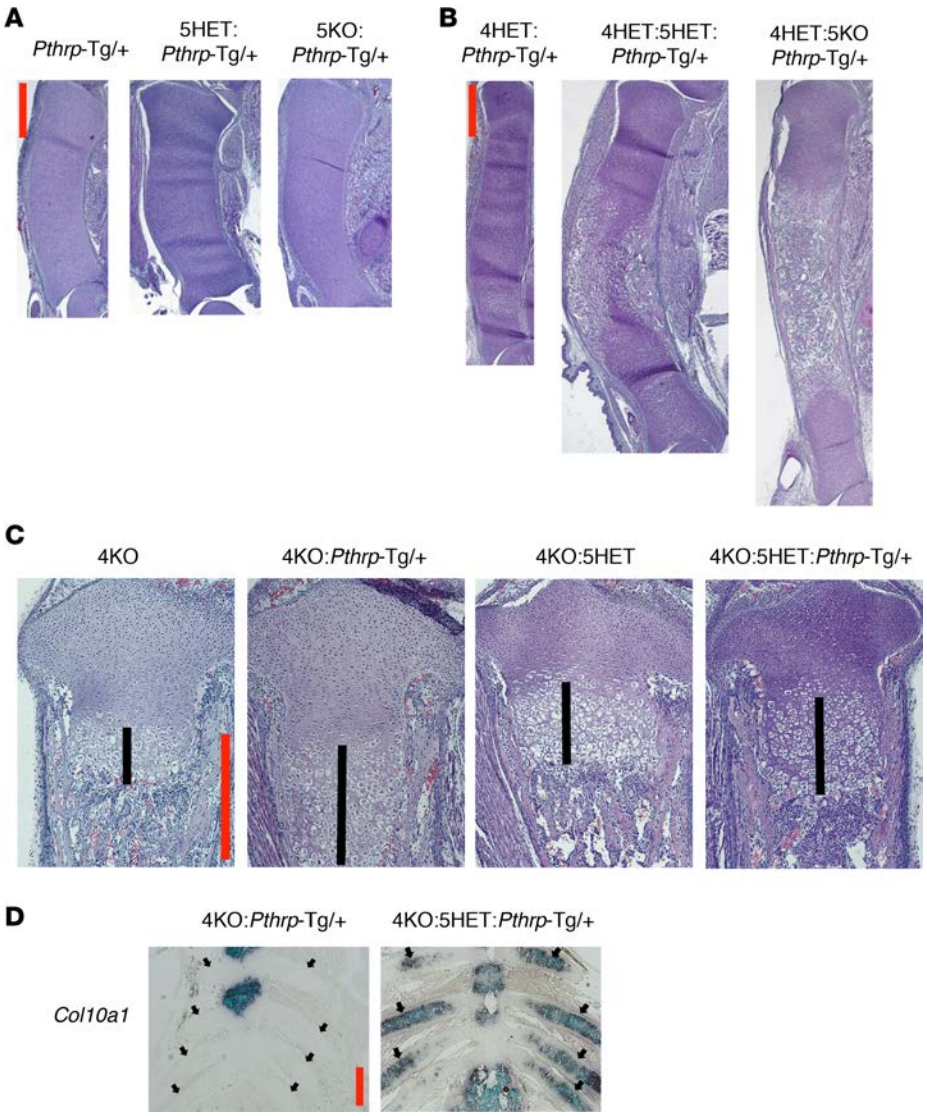

Figure 6. HDAC5 mediates PTHrP signaling when HDAC4 expression is low. (**A** and **B**) H&E staining of the whole tibia at birth (original magnification, ×20). The mice shown are littermates (**A**) or were born from the same parents (**B**). 4HET, *Hdac4*-HET. (**C**) H&E staining of the proximal tibial growth plate at birth (original magnification, ×100). The mice in the first and second images and those in the third and fourth images are littermates, respectively. Black lines indicate the length of hypertrophic chondrocyte layer. (**D**) ISH for *Col10a1* mRNA in the anterior rib cage at birth (original magnification, ×40). Black arrows in the image on the right indicate abnormal *Col10a1* mRNA expression in the anterior rib cartilage. *Col10a1* mRNA expression is not seen in the anterior rib cartilage in the image on the left (black arrows). Note that *Col10a1* mRNA expression seen on the left is in the sternum. The reproducibility of the phenotype was confirmed by 2 independent animals for each genotype. Scale bars (red lines): 500 μm.

HDAC4 expression limited, we found a stepwise acceleration of chondrocyte differentiation when the *Hdac4*-HET deletion was combined with the *Hdac5*-HET deletion and then the *Hdac5*-KO deletion (Figure 6B). We confirmed that the *Hdac4* and/or *Hdac5* deletions did not lower *Pthrp* mRNA overexpression (Supplemental Figure 6A). These results demonstrate that HDAC5 mediates PTHrP signaling, when the expression level of HDAC4 is low.

Further, we deleted the *Hdac5* gene in the *Hdac4*-KO: *Pthrp*-Tg/+ mouse. Tg expression of PTHrP in the *Hdac4*-KO: *Hdac5*-HET mouse had only a modest effect on the growth plate, in contrast to the differences between the *Hdac4*-KO mouse and the *Hdac4*-KO: *Pthrp*-Tg/+ mouse (Figure 6C). The *Hdac4* and *Hdac5* deletions did not lower *Pthrp* mRNA overexpression in this mouse model (Supplemental Figure 6B).

Importantly, we saw widespread *Col10a1* mRNA expression in rib chondrocytes in the *Hdac4*-KO: *Hdac5*-HET: *Pthrp*-Tg/+ mouse despite PTHrP overexpression (Figure 6D, black arrows on the right) in contrast to

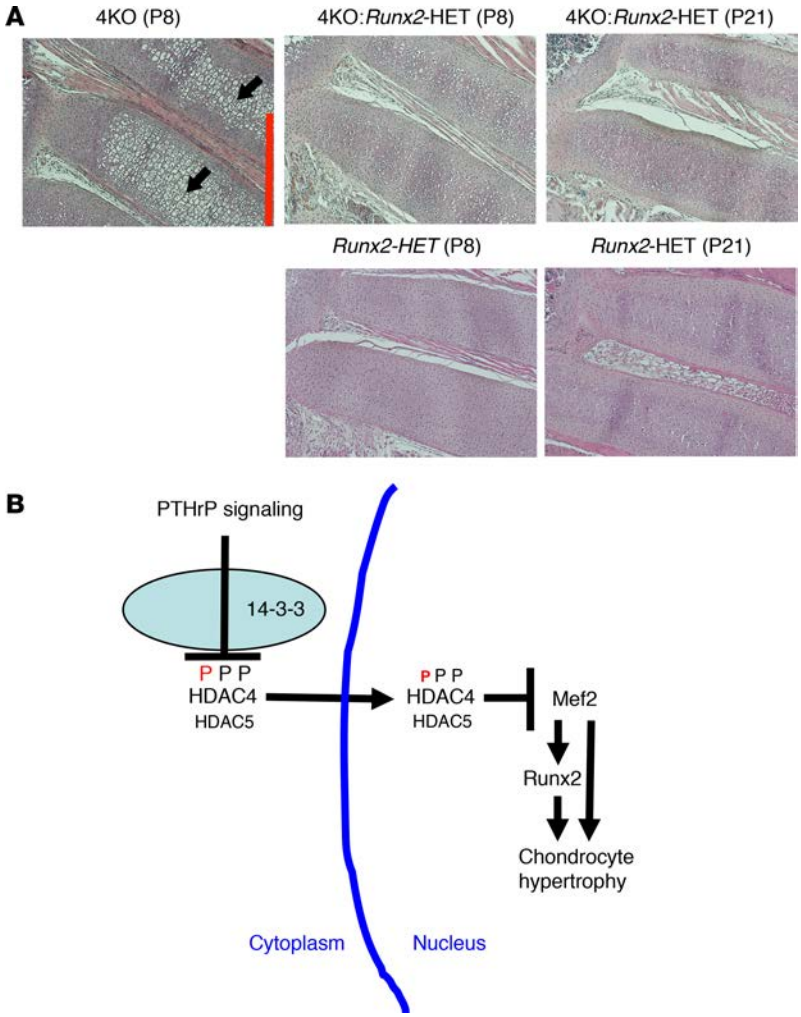

Figure 7. The Mef2/Runx2 signaling cascade is repressed by HDAC4/5 through PTHrP action. (**A**) H&E staining of the anterior rib cartilage at P8 and P21 (original magnification, ×100). Mice at the same age are littermates. The *Hdac4*-KO mice die between P10 and P14. Black arrows indicate abnormal rib chondrocyte hypertrophy, which is cancelled by HET deletion of *Runx2* (top images). Scale bar (red line): 500 μm. The *Runx2*-HET mouse exhibits normal rib phenotype (bottom images). (**B**) Proposed model for developmental regulation of chondrocyte hypertrophy. This model is derived from the data in this manuscript and those in previous reports (20, 21). PTHrP action increases HDAC4 nuclear translocation by decreasing phosphorylation of HDAC4 at the 14-3-3–binding sites. HDAC5 also mediates PTHrP signaling when HDAC4 expression is low. In the nucleus, HDAC4 and HDAC5 block the transcriptional activity of Mef2 through HDAC4/5's Mef2-binding sites. Mef2 drives chondrocyte hypertrophy both by direct activation and through activation of Runx2 expression. Runx2 works downstream of HDAC4/Mef2 and HDAC5/Mef2 to drive chondrocyte hypertrophy.

the absence of *Col10a1* mRNA expression in ribs of the *Hdac4*-KO: *Pthrp*-Tg/+ mouse (Figure 6D, left). We were unable to generate the *Hdac4*-KO: *Hdac5*-KO: *Pthrp*-Tg/+ mouse, given the small litter size in the *Pthrp*-Tg background mice. Taken together, these ISH data provide molecular evidence that HDAC5 is an essential mediator of PTHrP signaling to repress chondrocyte hypertrophy in the *Hdac4*-KO mouse.

The Mef2/Runx2 signaling cascade is activated when PTHrP/HDAC4 actions are low. A previous study demonstrated using ISH that the KO of *Mef2C* in chondrocytes and osteoblasts using *Twist2-Cre* led to lack of the normal increase in *Runx2* mRNA expression in the prehypertrophic region of the growth plates (20). This result suggests that Mef2C is required, either directly or indirectly, for *Runx2* expression, making *Runx2* expression a readout of and likely contributor to Mef2C action (29). We wondered whether Runx2, an essential transcription factor for differentiation of osteoblasts (30, 31) and chondrocytes (32), contributes to chondrocyte hypertrophy in our mouse models.

We examined the role of Runx2 in chondrocyte hypertrophy using the *Hdac4*-KO mouse. A previous report showed that, in the *Hdac4*-KO mice, *Hdac4* deletion leads to high Mef2C activity that subsequently induces rib chondrocyte hypertrophy and mineralization anteriorly, where this does not normally occur (20). At P8, the *Hdac4*-KO mice exhibited substantial chondrocyte hypertrophy, in that way resembling the *Pthrp*-KO mouse (Figure 1A and Figure 7A, black arrows). The HET deletion of *Runx2* in the *Hdac4*-KO mouse abrogated chondrocyte hypertrophy at P8 (Figure 7A, top middle), which enabled this mouse to survive longer with a normal rib phenotype (Figure 7A, top right). The HET deletion of *Runx2* itself had no effects on the rib phenotype (Figure 7A, bottom). This experiment, combined with previous experiments (20), indicates that Mef2 fails to induce chondrocyte hypertrophy when Runx2 expression is limited.

Figure 7B summarizes the model resulting from our data and the previous manuscripts (20, 21). PTHrP action increases HDAC4 nuclear translocation by decreasing phosphorylation of HDAC4 at the 14-3-3–

binding sites. HDAC5 also mediates PTHrP signaling when HDAC4 expression is low. In the nucleus, HDAC4 and HDAC5 block the transcriptional activity of Mef2 through the Mef2-binding sites. Mef2 drives chondrocyte hypertrophy both by direct action and by activating Runx2 expression. Runx2 works downstream of HDAC4/Mef2 and HDAC5/Mef2 to drive chondrocyte hypertrophy. Taken together, we reveal the main signaling pathway that regulates chondrocyte hypertrophy.

Discussion

During endochondral bone formation, chondrocyte hypertrophy is a crucial turning point in which the differentiation program is switched from chondrocyte differentiation to bone formation. Chondrocyte hypertrophy is also an important component of bone lengthening. Hypertrophic chondrocytes provide crucial signals for vascular invasion and osteoblast differentiation (1, 4, 5, 6). As seen in the perinatal lethality of the *Pthrp*-KO mice (10), chondrocyte hypertrophy must be regulated properly to maintain normal bone development. The molecular mechanisms used by PTHrP to inhibit chondrocyte hypertrophy in vivo have not been previously identified.

Previous work from our coauthors, Elena Kozhemyakina and Andrew Lassar, established an in vitro model that PTHrP rapidly leads to lower levels of phosphorylation of HDAC4 in cultured cells, in association with movement of HDAC4 to the nucleus, where HDAC4 then binds to Mef2C and blocks activation of a Mef2C target promoter (21). Here, we provide in vivo genetic evidence that HDAC4 is required for PTHrP action and that PTHrP action leads in vivo to underphosphorylation of HDAC4 and greater nuclear accumulation of HDAC4, with subsequent suppression of the expression of *Collagen 10a1*, a Mef2C and Runx2 target gene. Thus, the in vivo and in vitro data together strongly support the hypothesis that HDAC4 mediates PTHrP signaling in chondrocytes. Further, the in vivo data show that HDAC4 is not the sole mediator of PTHrP action. We found that, though the *Hdac5*-KO mouse does not have a bone phenotype at birth, HDAC5 is needed to mediate the action of PTHrP when HDAC4 is decreased or missing (Figure 6, B–D). We did not analyze *Hdac4* and *Hdac7* double-mutant mice to examine if HDAC7 also mediates PTHrP signaling. PTHrP signaling lowers the level of phosphorylation of the first 14-3-3–binding site of HDAC7 (Figure 3, A and C, and Supplemental Figure 4A), suggesting that PTHrP also lowers HDAC7 phosphorylation. However, HDAC7 alone cannot block accelerated chondrocyte hypertrophy in the *Hdac*4 and *Hdac5* double-KO mouse at birth (Figure 5 and Supplemental Figure 5, A and B). In contrast, HDAC5 can block accelerated chondrocyte hypertrophy in the *Hdac4*-KO mouse at birth (Figure 5). Thus, we concluded that HDAC4 and HDAC5 are the main mediators of PTHrP signaling in chondrocytes; we cannot exclude a role of HDAC7 as well.

We show that PTHrP signaling lowers phosphorylation of the 14-3-3–binding sites of HDAC4, particularly at residue Ser245 (Figure 3, A–D, and Supplemental Figure 4A), and increases nuclear localization of HDAC4 (Figure 3, E and F). An in vitro study using cultured chick primary chondrocytes provided evidence that PTHrP signaling activates protein phosphatase 2A (PP2A), a phosphatase that targets HDAC4-Ser245 (21). We attempted to examine the role of PP2A, using metatarsal explants from the newborn *Pthrp*-Tg/+ mice treated with okadaic acid, to see if this PP2A inhibitor could stimulate chondrocyte hypertrophy as it stimulates *Col10a1* mRNA expression in the in vitro study (21). Unfortunately, okadaic acid was too toxic to the metatarsal explants to allow clear interpretation of results. Salt-inducible kinase 3 (Sik3) influences chondrocyte hypertrophy; the Sik3-KO mouse exhibits delay in chondrocyte hypertrophy (33). An in vitro study analyzing overexpressed proteins in HEK293T cells demonstrated that Sik2 and Sik3 phosphorylate the 14-3-3–binding sites of HDAC4 and HDAC5 (34). Further work will be needed to determine whether PTHrP regulates the phosphorylation of HDAC4 and HDAC5 by regulating kinases or phosphatases or both in vivo.

Further, we investigated mediators working downstream of the PTHrP/HDAC4/Mef2 pathway. A previous study showed that Runx2 mRNA expression is reduced in the prehypertrophic region of the growth plate when Mef2C was knocked out of chondrocytes and osteoblasts using *Twist2-Cre*, a finding consistent with the idea that, in chondrocytes, Runx2 expression reflects Mef2 action (20). To test if Runx2 drives chondrocyte hypertrophy downstream of Mef2, we utilized the *Hdac4*-KO mouse as a genetic model for this functional analysis. In the *Hdac4*-KO mouse, higher Mef2 action by homozygous *Hdac4* deletion leads to extensive rib chondrocyte hypertrophy, including in regions that do not normally become hypertrophic (Figure 1, B and D, and Figure 7A). When the *Hdac4*-KO mouse was also made HET for *Runx2*, chondrocyte hypertrophy was completely blocked (Figure 7A). This result indicates the need for Runx2 expression to activate differentiation into hypertrophic chondrocytes in this setting.

Chondrocyte hypertrophy is regulated by the balance between transcriptional activation by Mef2C and repression by HDAC4 in the nucleus (20). Using in vivo animal models, we demonstrated that a key determinant in this system is that PTHrP regulates the nuclear translocation of HDAC4. When PTHrP action is low, the lower nuclear distribution of HDAC4 allows Mef2 to increase *Runx2* mRNA expression that subsequently induces chondrocyte hypertrophy.

The *Pthrp*-Tg/+ mouse is an animal model for chondrodysplasia characterized by short-limbed dwarfism (13). In humans, Jansen-type metaphyseal chondrodysplasia, a rare form of short-limbed dwarfism, is caused by a constitutively active mutant PTH/PTHrP receptor (35). In the present study, the delayed chondrocyte development in the *Pthrp*-Tg/+ mouse can be rescued by HET or homozygous deletion of *Hdac4* (Figure 2B) or double-HET deletion of *Hdac4* and *Hdac5* (Figure 6B). HDAC4 and/or HDAC5 would be potential therapeutic targets for Jansen-type metaphyseal chondrodysplasia. Further, the brachydactyly exhibited by people with heterozygosity for expression of PTHrP (22), Gs α (36), or HDAC4 (23) suggests that the pathway analyzed here controls growth plate function in humans as well.

In this study, we provide in vivo genetic evidence to reveal the downstream mediators of PTHrP signaling in chondrocytes. We expect that our genetic and molecular analyses of the bones in vivo provide a possible molecular mechanism of PTHrP signaling that might contribute to actions of PTHrP in other target organs, such as teeth, mammary glands, skin and hair, blood vessels, placenta, and pancreas (37).

Methods

Mutant mice. The *Pthrp* universal KO mouse was generated by our group (10). The other mutant mice were generated and provided as follows: *Hdac4* universal KO mouse (19), *Hdac4*-floxed mouse (25), and *Hdac5* universal KO mouse (16) from E. Olson and R. Bassel-Duby (University of Texas Southwestern Medical Center, Dallas, Texas, USA); *Col2*-promoter: *Pthrp*-Tg mouse (13) from A. Broadus (Yale University, New Haven, Connecticut, USA); *Col2-Cre* mouse (24) from R. Behringer (University of Texas MD Anderson Cancer Center, Houston, Texas, USA); *Osx-Cre-GFP* mouse (26) from A. McMahon (Keck School of Medicine, University of Southern California, Los Angeles, USA); and *Runx2* universal KO mouse (31) from M. Owen (Imperial Cancer Research Fund, London, United Kingdom). Each genotype was confirmed by PCR primers shown in Supplemental Table 2A.

Each mutant mouse was backcrossed to the C57BL/6 WT mice (Charles River, strain code 027) for at least 10 generations. The mice were housed in the Center for Comparative Medicine at the Massachusetts General Hospital (MGH), with regular food and water, under regular housing conditions.

Antibodies. HDAC4 rabbit polyclonal antibody (Abcam, ab12172), Phospho-HDAC4 (Ser246)HDAC5 (Ser259)/HDAC7 (Ser155) rabbit mAb (Cell Signaling, 3443), Phospho-HDAC4 (Ser467) rabbit polyclonal antibody (27) (generated by T.P. Yao), Phospho-HDAC4 (Ser632) rabbit polyclonal antibody (Santa Cruz, sc-101691), β-actin rabbit mAb (Cell Signaling, 8457), Rabbit IgG-HRP goat secondary antibody (Santa Cruz, sc-2004), DIG-AP, Fab fragments sheep polyclonal antibody (Roche, 11093274910), Rabbit IgG (H+L), and Alexa Fluor 488 goat secondary antibody (Life Technologies, A11008).

Histology. We used formalin-fixed paraffin sections for the histological experiments in this study (H&E staining, ISH, and IHC). We fixed hind limbs and rib cages with 3.7% formaldehyde (MilliporeSigma, 252549)/PBS (pH 7.4) at 4°C for 2 days. Then, we decalcified the samples with 15% EDTA (pH 7.4) (MilliporeSigma, E9884) at 4°C for 1 day (E17.5, E18.5, and P0), 1 week (P8, P12), or 2 weeks (P21). After the paraffin processing and embedding, we cut 6-μm sections onto Superfrost Plus Microscope Slides (Thermo Fisher, 12-550-20). Before each histological experiment, the slides were baked at 58°C for 30 minutes, deparaffinized by xylene (5 minutes for 3 times), and then rehydrated by ethanol (2 minutes in 100% ethanol for 2 times and then 2 minutes in 95% ethanol).

ISH. DIG-labeled complementary RNA (cRNA) probes were synthesized using DIG RNA–labeling mix (Roche, 11277073910) with T7 RNA polymerase (Roche, 10881767001) or SP6 RNA polymerase (Roche, 10810274001) according to the manufacture's protocol. After DNase (Promega, M6101) treatment and subsequent ethanol precipitation using LiCl (MilliporeSigma, L9650), we resuspended the cRNA pellet in 100 μl RNase-free water. The target regions of the cRNA probes are listed in Supplemental Table 2B.

For day 1 (pretreatment and hybridization), we modified a previously described protocol (38). After baking, deparaffinization, and rehydration, the sections were subjected to fixation using 4% paraformaldehyde (PFA, Thermo Fisher, 416785000) for 10 minutes at room temperature, Proteinase K treatment (Thermo Fisher, 17916; 3 μg/ml in PBS, pH 7.4) for 10 minutes at room temperature, post-fixation by 4%

PFA for 5 minutes at room temperature, and acetylation for 10 minutes at room temperature using 0.25% acetic acid and 0.1 M Triethanolamine (MilliporeSigma, A6404 and T1377) in Milli-Q water. Each step was followed by 2 PBS washes for 5 minutes. After the last PBS wash, the slides were immersed in 80% ethanol for 3 minutes and then air-dried briefly. We used 0.5 μl DIG-labeled cRNA probe per a slide with 300 μl hybridization buffer (50% Formamide [MilliporeSigma, F9037], 10 mM Tris [pH 8.0], 200 μg/ml yeast tRNA [MilliporeSigma, R8759], 1× Denhardt's solution [MilliporeSigma, D2532], 10% Dextran sulfate [MilliporeSigma, D8906], 600 mM NaCl, 0.25% SDS, 1 mM EDTA [pH 8.0]). We incubated the slides with glass coverslips in a moist slide box (with 50% Formamide in 5× saline-sodium citrate [SSC] at the bottom) at 58°C for overnight.

For day 2 (washing and antibody incubation), we followed a previously described protocol (39), except we added a blocking step. After washing sequentially with SSC (2× SSC at room temperature for 30 minutes, 2× SSC at 60°C for 1 hour, and then 0.2× SSC at 60°C for 1 hour), we blocked the slides at room temperature for 1 hour using 5% heat inactivated sheep serum (MilliporeSigma, S3772) and 5% Blocking Reagent (Roche, 11096176001) in 100 mM Tris (pH 7.5)/150 mM NaCl buffer. Then, we incubated the slides with anti-DIG-AP antibody (1:2,500 dilution by the blocking buffer) at room temperature for 2 hours. After 2 washes with 100 mM Tris (pH 7.5)/150 mM NaCl buffer for 15 minutes and a subsequent wash with 100 mM Tris (pH 9.5)/100 mM NaCl/50 mM $MgCl_2$ buffer for 10 minutes, we incubated the sides with BM-Purple (Roche, 11442074001) at room temperature for 1–4 days until visible signals could be observed. We mounted the slides with Aqua-Mount Slide Mounting Media (Thermo Fisher, 13800) after fixing the slides with 4% PFA in PBS (pH 7.4) at room temperature for 30 minutes and washing subsequently by PBS.

Manual microdissection. We modified the protocol shown in ref. 40. Hind limbs were embedded in O.C.T. compound (Sakura Finetek USA, 4583) on dry ice without fixation. The blocks were stored at –80°C until cryosectioning by Shandon Cryostat. We attached 4–6 cryosections (40-μm thick) on Superfrost Plus Microscope Slides and kept the slides in ice-cold 70% ethanol. After washing in Milli-Q water for 30 seconds, we stained a slide with 10% Harris Hematoxylin (Thermo Fisher, 245-677) for 30 seconds. After we washed the slide in Milli-Q water for 30 seconds, we immersed the slide in 3% glycerol solution (Thermo Fisher, BP-229-1) to keep the sections wet during manual microdissection. We placed a slide on a petri dish filled with ice and dissected the proximal tibial growth plates using 28-gauge needle under a dissecting microscope. Dissected sections were collected in Buffer RLT (Qiagen, RNeasy Mini Kit, 74104) for microarray analysis or in 4× Laemmli SDS sample buffer (Boston Bioproducts, BP-110R) for Western blot. To prepare 1 sample, we dissected 18–20 tibiae from the same litter for microarray analysis and 2 tibiae from the same mouse for Western blot.

Western blot. After freeze and thaw for 4 cycles (liquid nitrogen, 37°C water, and vortex for 1 minute) and subsequent sonication (intermittently for 20 seconds, twice), the whole cell lysates were separated by 10% SDS-PAGE gel (Expedeon, NXG01012 or NXG01027). We transferred the gel to a Hybond ECL nitrocellulose membrane (Amersham, RPN303D) at 120 V for 1.5 hours. After blocking with 5% BSA (Boston Bioproducts, P-753) in TBS-T (Tris-buffered saline with TWEEN 20, 50 mM Tris [pH 7.5], 150 mM NaCl, 0.05% TWEEN 20 [MilliporeSigma, P9416]) at room temperature for 1 hour, we incubated the membrane in a sealer bag with primary antibody (1:1,000–3,000 dilution by the blocking solution) on a shaker at 4°C for overnight. After washing the membranes in TBS-T (10 minutes, 4 times), we incubated the membrane with secondary antibodies (1:5,000 dilution by TBS-T) at room temperature for 1 hour. After washing in TBS-T (10 minutes, 4 times), we incubated the membranes with ECL (Enhanced Chemi Luminescence) substrate (Thermo Fisher, 32109) at room temperature for 1 minute. We detected the signals by autoradiographic film (Lab Scientific, AR-ALF-2025). We analyzed the band intensities using Image Studio Lite version 5.0 (LI-COR Biotechnology).

IHC. We modified a protocol by Abcam (http://www.abcam.com/ps/pdf/protocols/ihc_p.pdf). After baking, deparaffinization, and rehydration, we retrieved antigens by boiling slides in a microwave oven for 10 minutes in 10 mM Tris/1 mM EDTA/0.05% TWEEN 20 (pH 9.0) buffer. After washing in running tap water for 5 minutes, we incubated slides with Protein Block (Abcam, ab64226) at room temperature for 1 hour. Then, we incubated slides at 4°C for overnight with anti-HDAC4 antibody (1:2,500 dilution by Antibody Diluent; Abcam, ab64211).

After washing with PBS 3 times, we incubated slides with Alexa Fluor 488 secondary antibody (1:400 dilution by Antibody Diluent) at room temperature for 2 hours. After washing with PBS, we stained with Cellomics Whole Cell Stains Red (Thermo Fisher, 8403401: 1:100 dilution by PBS) at room temperature for

30 minutes. After washing with PBS, we stained the slides with 300 nM DAPI (MilliporeSigma, D9542) at room temperature for 10 minutes and then washed with PBS for 3 times. We mounted the slides with Prolong Gold Antifade Reagent (Life Technologies, P36930) and no. 1.5 glass coverslips (Thermo Fisher, 12-544-E).

Confocal microscopy. We used the Zeiss LSM 510 Confocal Microscope system (a 488-nm argon ion laser for Alexa Fluor 488, a 405-nm diode laser for DAPI, a 633-nm Helium-Neon laser for Whole Cell Stain), with a ×63 oil objective lens, to observe fluorescent signals by IHC. We reduced the background signals by scanning sections using a small pinhole (8 μm). We used higher laser power to compensate the lower signal intensities associated with the small pinhole.

Microarray analysis. Affymetrix GeneChip analysis was performed using total RNA obtained by manual microdissection from the 3 layers of the proximal tibial growth plates in the newborn Black Swiss WT mice (Taconic). Total RNA was extracted using the RNeasy Mini Kit (Qiagen, 74104) with QIAshredder (Qiagen, 79654) and on-column DNase I treatment (Qiagen, 79254). The first-strand cDNA, the second-strand cDNA, and the biotin-labeled cRNA were synthesized by the GeneChip One Cycle Target Labeling kit (Affymetrix, 900493). After the cRNA fragmentation, we hybridized onto a GeneChip Mouse Genome 430 2.0 Array using the Affymetrix GeneChip Operating System. Biological triplicate data were normalized and combined using Rosetta Resolver software (Rosetta Biosoftware). The total data sets for the microarray analysis have been deposited in the Gene Expression Omnibus (GSE87605).

Quantitative analysis of the confocal images. To calculate the total HDAC4 signal intensities in nuclei and those in whole cells on the immunohistochemical images, we analyzed the intensities of 3 colors (HDAC4, DAPI, and whole cell stain) using image analyzing software, Volocity (PerkinElmer). We prepared paraffin sections of tibiae from 5 sets of the *Pthrp*-KO mice and the *Pthrp*-Tg/+ mice at birth. For each set of animals, we processed IHC and confocal microscopy together on the same dates. We captured multiple images from different areas in the round chondrocyte regions in the proximal tibial growth plate (6–17 images per each mouse). Each image has 80–120 cells that were scanned at random levels by the confocal plane. We assigned the total sum of HDAC4 signals in the HDAC4 and DAPI double-positive areas as the HDAC4 signal in the nuclear compartments in each image. Similarly, we assigned the total sum of HDAC4 signals in the HDAC4 and whole cell stain double-positive areas as the HDAC4 signal in the whole cellular compartments. To determine the threshold signal intensity for the positive area, we calculated the average background signal intensities in the extracellular regions. To calculate signal intensities in the double-positive areas, we used the intersect function of Volocity. We obtained similar average ratios of HDAC4 in nuclei versus whole cells by analyzing 5, 10, and 15 images from the same animal. Thus, we could get representative average ratios by analyzing at least 5 images (including 400–500 cells).

Statistics. For Figure 1, A–C, we prepared 3 independent animals for each genotype (n = 3, biological triplicate). We measured the average length of the proliferating chondrocyte region using 9 different sections for each mouse. We compared the measurement of each genotype to that of its corresponding WT genotype with the 2-tailed Student's t test. A P value of less than 0.05 was considered significant.

For Figure 2A, we prepared 3 independent newborn litters that included every genotype (WT, *Hdac4*-HET, *Pthrp*-HET, and *Hdac4* and *Pthrp* double HET) in the littermates (n = 3, biological triplicate). We measured the length of the proliferating chondrocyte region (shown by black lines in Figure 2A) on 9 different sections for each mouse. Twenty-seven measurements from sections of each mouse were analyzed using a random intercept linear mixed-effects model (SAS Institute), a method to analyze multiple measurements with consideration of fixed effects and mixed effects. A P value of less than 0.05 was considered significant.

For Figure 3B, we prepared 3 sets of the *Pthrp*-Tg/+ mice, WT mice, and the *Pthrp*-KO mice at birth (n = 3, biological triplicate). We performed a Western blot for these 9 samples on the same gel (Figure 3A) to calculate the band intensities. HDAC4 was normalized to β-actin, and phosphorylated HDAC4 proteins were normalized to total HDAC4. We compared the measurement of each genotype to that of the WT genotype by the 2-tailed Student's t test. A P value of less than 0.05 was considered significant.

For Figure 3D, we prepared 4 sets of the *Pthrp*-Tg/+ mice and the *Pthrp*-KO mice at birth (n = 4, biological replicate). We performed 2 independent Western blots for 4 samples (Figure 3C and Supplemental Figure 4A) to calculate the band intensities. We also performed a Western blot for 8 samples on the same gel using β-actin antibody to adjust protein loading of the two different gels. HDAC4 was normalized to β-actin, and phosphorylated HDAC4 proteins were normalized to total HDAC4. Each P value was calculated using the 2-tailed Student's t test with Bonferroni correction. A P value of less than 0.05 was considered significant.

For Figure 3F, we prepared 5 sets of the *Pthrp*-Tg/+ mice and the *Pthrp*-KO mice at birth ($n = 5$, biological replicate). We captured multiple confocal images from different areas for each animal. We calculated the average ratios of the total nuclear HDAC4 to the total cellular HDAC4 for each image (Supplemental Figure 4B and Supplemental Table 1). Individual data for each animal were analyzed by the mixed-effects model described above for Figure 2A. A P value of less than 0.05 was considered significant.

Study approval. All animal experiments were approved by the Institutional Animal Care and Use Committee (IACUC) at MGH. We performed all the mouse procedures in accordance with the IACUC regulations and guidelines.

Author contributions

SN, EK, ABL, and HMK designed research studies. SN, TK, and HMK designed the methodology. SN, FL, and MS conducted the experiments. SN acquired and analyzed data. TPY provided a reagent (phospho-HDAC4 [Ser467] antibody). SN and HMK wrote the original manuscript. SN, TK, ABL, and HMK reviewed the manuscript. SN and HMK edited the final manuscript. HMK acquired funding. HMK provided study supervision.

Acknowledgments

We thank E. Olson and R. Bassel-Duby for providing the class IIa HDAC-KO mice and for advising regarding these mice. We thank M. Wein for reading the manuscript carefully. We thank N. Ono, D. Balani, E. Williams, and other members of Kronenberg lab for helpful collaborations. We also thank members of Tabin program project (C. Tabin and lab members; A. McMahon and lab members; advisors: B. Olsen, V. Rosen, M. Warman, G. Karsenty, B. Horton, and A. Broadus) for thoughtful discussions. We thank T. Diefenbach (Ragon Institute of MGH, MIT and Harvard) for help with the confocal microscopy; D. Brown and R. Bouley (MGH Center for Systems Biology) for help with the confocal image analysis using PerkinElmer Volocity; H. Lee (MGH Biostatistics Center) for help with the statistical analysis; J. Couget, R. Gali, and P. Grosu (FAS Center for Systems Biology at Harvard University) for help with the Affymetrix microarray and data analysis; and M. Demay, L. Cai, and D. Hu (MGH Center for Skeletal Research) for the paraffin processing. This work was supported by NIH grants DK 56246, DK011794, and P30 AR066261 to HMK.

Address correspondence to: Henry M. Kronenberg, Endocrine Unit, Massachusetts General Hospital, 50 Blossom Street, Their 1101, Boston, Massachusetts 02114, USA. Phone: 617.726.3967; Email: hkronenberg@mgh.harvard.edu.

1. Kronenberg HM. Developmental regulation of the growth plate. *Nature*. 2003;423(6937):332–336.
2. Chung UI, Schipani E, McMahon AP, Kronenberg HM. Indian hedgehog couples chondrogenesis to osteogenesis in endochondral bone development. *J Clin Invest*. 2001;107(3):295–304.
3. Kobayashi T, et al. PTHrP and Indian hedgehog control differentiation of growth plate chondrocytes at multiple steps. *Development*. 2002;129(12):2977–2986.
4. Ono N, Ono W, Nagasawa T, Kronenberg HM. A subset of chondrogenic cells provides early mesenchymal progenitors in growing bones. *Nat Cell Biol*. 2014;16(12):1157–1167.
5. Ono N, Ono W, Mizoguchi T, Nagasawa T, Frenette PS, Kronenberg HM. Vasculature-associated cells expressing nestin in developing bones encompass early cells in the osteoblast and endothelial lineage. *Dev Cell*. 2014;29(3):330–339.
6. Maes C, et al. Osteoblast precursors, but not mature osteoblasts, move into developing and fractured bones along with invading blood vessels. *Dev Cell*. 2010;19(2):329–344.
7. Albright F. Case records of the Massachusetts General Hospital–Case 27461. *N Engl J Med*. 1941; 225(20):789–791.
8. Suva LJ, et al. A parathyroid hormone-related protein implicated in malignant hypercalcemia: cloning and expression. *Science*. 1987;237(4817):893–896.
9. Jüppner H, Abou-Samra AB, Uneno S, Gu WX, Potts JT, Segre GV. The parathyroid hormone-like peptide associated with humoral hypercalcemia of malignancy and parathyroid hormone bind to the same receptor on the plasma membrane of ROS 17/2.8 cells. *J Biol Chem*. 1988;263(18):8557–8560.
10. Karaplis AC, et al. Lethal skeletal dysplasia from targeted disruption of the parathyroid hormone-related peptide gene. *Genes Dev*. 1994;8(3):277–289.
11. Lanske B, et al. PTH/PTHrP receptor in early development and Indian hedgehog-regulated bone growth. *Science*. 1996;273(5275):663–666.
12. Jobert AS, et al. Absence of functional receptors for parathyroid hormone and parathyroid hormone-related peptide in Blomstrand chondrodysplasia. *J Clin Invest*. 1998;102(1):34–40.
13. Weir EC, Philbrick WM, Amling M, Neff LA, Baron R, Broadus AE. Targeted overexpression of parathyroid hormone-related peptide in chondrocytes causes chondrodysplasia and delayed endochondral bone formation. *Proc Natl Acad Sci USA*.

1996;93(19):10240–10245.
14. Haberland M, Montgomery RL, Olson EN. The many roles of histone deacetylases in development and physiology: implications for disease and therapy. *Nat Rev Genet*. 2009;10(1):32–42.
15. Grozinger CM, Schreiber SL. Regulation of histone deacetylase 4 and 5 and transcriptional activity by 14-3-3-dependent cellular localization. *Proc Natl Acad Sci USA*. 2000;97(14):7835–7840.
16. Chang S, McKinsey TA, Zhang CL, Richardson JA, Hill JA, Olson EN. Histone deacetylases 5 and 9 govern responsiveness of the heart to a subset of stress signals and play redundant roles in heart development. *Mol Cell Biol*. 2004;24(19):8467–8476.
17. Chang S, Young BD, Li S, Qi X, Richardson JA, Olson EN. Histone deacetylase 7 maintains vascular integrity by repressing matrix metalloproteinase 10. *Cell*. 2006;126(2):321–334.
18. Zhang CL, McKinsey TA, Chang S, Antos CL, Hill JA, Olson EN. Class II histone deacetylases act as signal-responsive repressors of cardiac hypertrophy. *Cell*. 2002;110(4):479–488.
19. Vega RB, et al. Histone deacetylase 4 controls chondrocyte hypertrophy during skeletogenesis. *Cell*. 2004;119(4):555–566.
20. Arnold MA, et al. MEF2C transcription factor controls chondrocyte hypertrophy and bone development. *Dev Cell*. 2007;12(3):377–389.
21. Kozhemyakina E, Cohen T, Yao TP, Lassar AB. Parathyroid hormone-related peptide represses chondrocyte hypertrophy through a protein phosphatase 2A/histone deacetylase 4/MEF2 pathway. *Mol Cell Biol*. 2009;29(21):5751–5762.
22. Klopocki E, et al. Deletion and point mutations of PTHLH cause brachydactyly type E. *Am J Hum Genet*. 2010;86(3):434–439.
23. Williams SR, et al. Haploinsufficiency of HDAC4 causes brachydactyly mental retardation syndrome, with brachydactyly type E, developmental delays, and behavioral problems. *Am J Hum Genet*. 2010;87(2):219–228.
24. Ovchinnikov DA, Deng JM, Ogunrinu G, Behringer RR. Col2a1-directed expression of Cre recombinase in differentiating chondrocytes in transgenic mice. *Genesis*. 2000;26(2):145–146.
25. Potthoff MJ, et al. Histone deacetylase degradation and MEF2 activation promote the formation of slow-twitch myofibers. *J Clin Invest*. 2007;117(9):2459–2467.
26. Rodda SJ, McMahon AP. Distinct roles for Hedgehog and canonical Wnt signaling in specification, differentiation and maintenance of osteoblast progenitors. *Development*. 2006;133(16):3231–3244.
27. Cohen TJ, et al. The histone deacetylase HDAC4 connects neural activity to muscle transcriptional reprogramming. *J Biol Chem*. 2007;282(46):33752–33759.
28. Lanske B, et al. The parathyroid hormone (PTH)/PTH-related peptide receptor mediates actions of both ligands in murine bone. *Endocrinology*. 1998;139(12):5194–5204.
29. Kawane T, et al. Dlx5 and mef2 regulate a novel runx2 enhancer for osteoblast-specific expression. *J Bone Miner Res*. 2014;29(9):1960–1969.
30. Komori T, et al. Targeted disruption of Cbfa1 results in a complete lack of bone formation owing to maturational arrest of osteoblasts. *Cell*. 1997;89(5):755–764.
31. Otto F, et al. Cbfa1, a candidate gene for cleidocranial dysplasia syndrome, is essential for osteoblast differentiation and bone development. *Cell*. 1997;89(5):765–771.
32. Yoshida CA, et al. Runx2 and Runx3 are essential for chondrocyte maturation, and Runx2 regulates limb growth through induction of Indian hedgehog. *Genes Dev*. 2004;18(8):952–963.
33. Sasagawa S, et al. SIK3 is essential for chondrocyte hypertrophy during skeletal development in mice. *Development*. 2012;139(6):1153–1163.
34. Walkinshaw DR, et al. The tumor suppressor kinase LKB1 activates the downstream kinases SIK2 and SIK3 to stimulate nuclear export of class IIa histone deacetylases. *J Biol Chem*. 2013;288(13):9345–9362.
35. Schipani E, Kruse K, Jüppner H. A constitutively active mutant PTH-PTHrP receptor in Jansen-type metaphyseal chondrodysplasia. *Science*. 1995;268(5207):98–100.
36. Pereda A, et al. Brachydactyly E: isolated or as a feature of a syndrome. *Orphanet J Rare Dis*. 2013;8:141.
37. McCauley LK, Martin TJ. Twenty-five years of PTHrP progress: from cancer hormone to multifunctional cytokine. *J Bone Miner Res*. 2012;27(6):1231–1239.
38. Murtaugh LC, Chyung JH, Lassar AB. Sonic hedgehog promotes somitic chondrogenesis by altering the cellular response to BMP signaling. *Genes Dev*. 1999;13(2):225–237.
39. Braissant O, Wahli WA. Simplified in situ hybridization protocol using non-radioactively labeled probes to detect abundant and rare mRNAs on tissue sections. *BIOCHEMICA*. 1998; 1:10–16.
40. Becker B, et al. Manual Microdissection. In: Bowtell D, Sambrook J, eds. *DNA Microarrays*. New York, NY: Cold Spring Harbor Laboratory Press; 2003: 316–318.